

Electronic Supplementary Information

Tunable Metal-Organic Framework Nanoarrays on Carbon Cloth Constructed by a Rational Self-Sacrificing Template for Efficient and Robust Oxygen Evolution Reaction

Chong Lin^a, Xiao He^a, Huiqin Li^{b*}, Junjie Zou^a, Miaoling Que^c, Jingyang Tian^{a*},
Yong Qian^{a*}

^a Jiangxi Province Key Laboratory of Polymer Micro/Nano Manufacturing and Devices, School of Chemistry, Biology and Materials Science, East China University of Technology, Nanchang, 330013, P. R. China.

^b Department of Chemistry and Chemical Engineering, Baoji University of Arts and Sciences, Shaanxi Key Laboratory of phytochemistry, Baoji, 721013, P. R. China.

^c School of Electronic and Information Engineering, Suzhou University of Science and Technology, Suzhou 215009, P. R. China.

Corresponding author: huiqinli@yeah.net (Prof. Li); jytian@ecut.edu.cn (Dr. Tian); yqian@ecut.edu.cn (Prof. Qian).

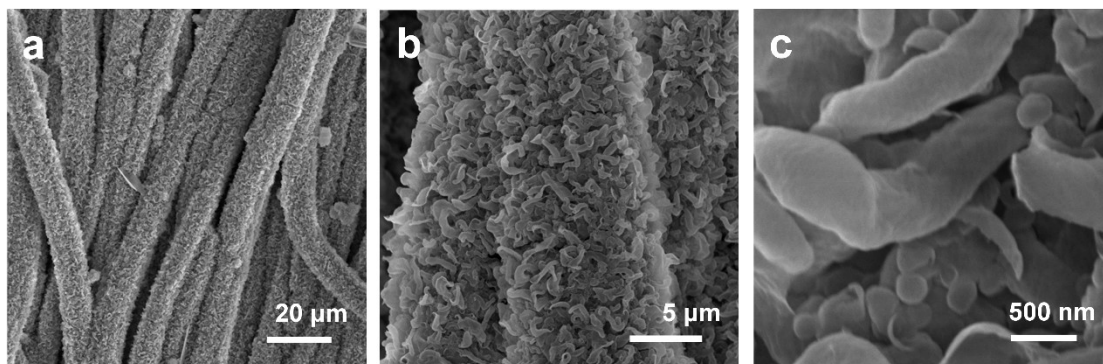


Figure S1. SEM images of Ni(OH)₂ NAs/CC.

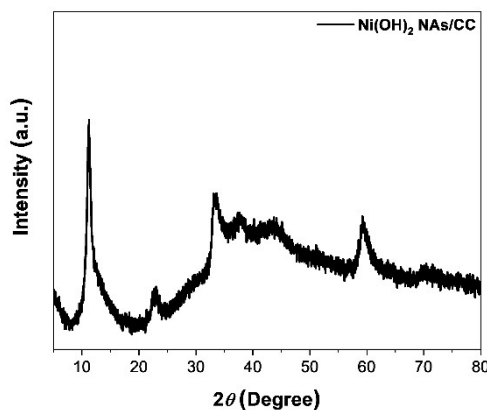


Figure S2. XRD of Ni(OH)₂ NAs/CC.

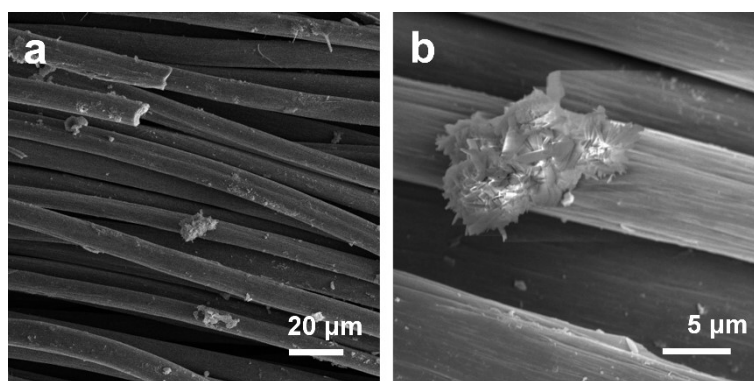


Figure S3. SEM images of Ni-MOF-74/CC without the template of Ni(OH)₂ NAs/CC.

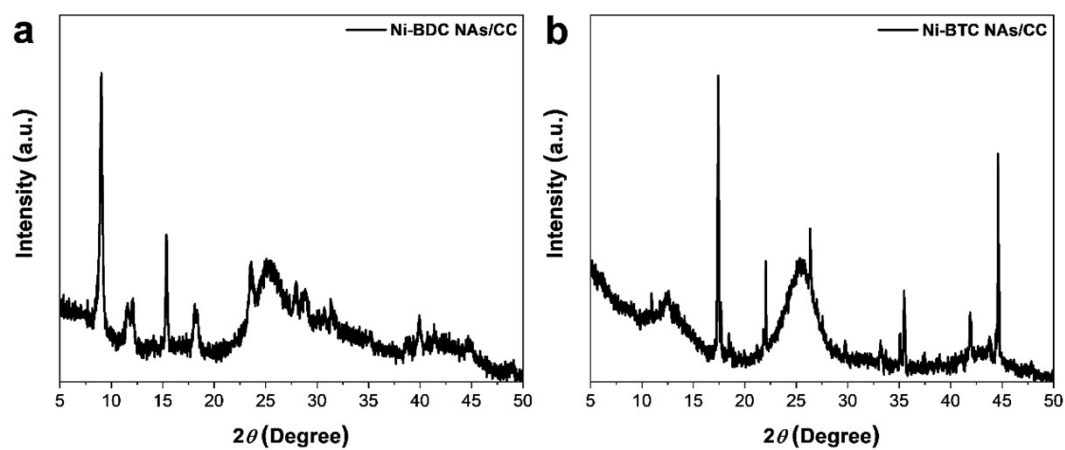


Figure S4. XRD patterns of (a) Ni-BDC NAs/CC and (b) Ni-BTC NAs/CC, respectively.

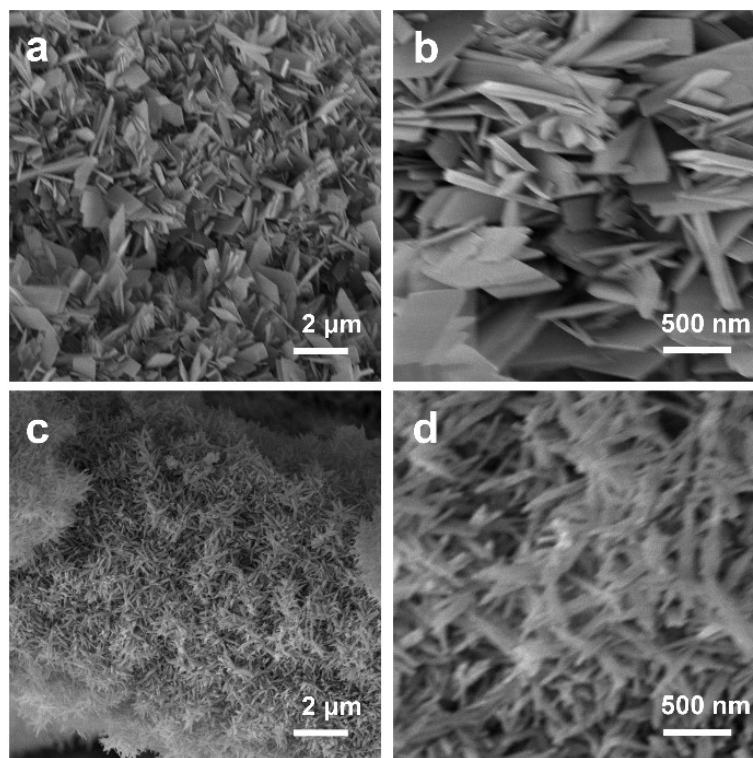


Figure S5. SEM images of (a, b) Ni-BDC NAs/CC and (c, d) Ni-BTC NAs/CC,

respectively.

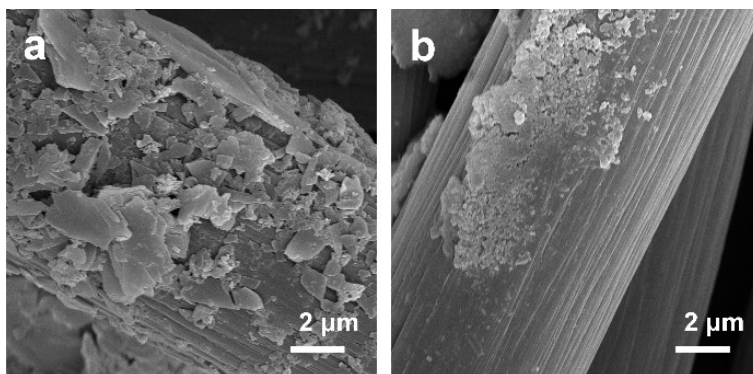


Figure S6. SEM images of (a) Ni-BDC/CC and (b) Ni-BTC/CC without the template of Ni(OH)₂ NAs/CC, respectively.

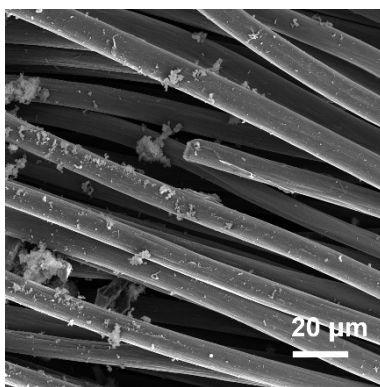


Figure S7. SEM image of Ni-MOF-74 NAs/CC-1 prepared with the addition of HAC (pH=3.06).

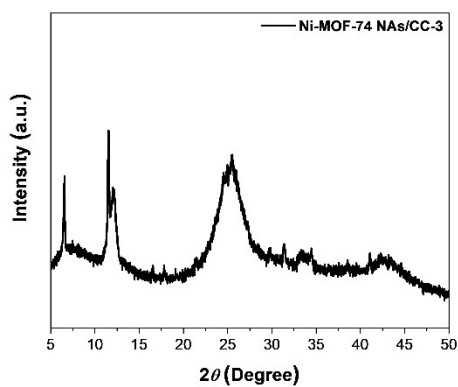


Figure S8. XRD pattern of Ni-MOF-74 NAs/CC-3 prepared with the addition of HMT (pH=3.45).

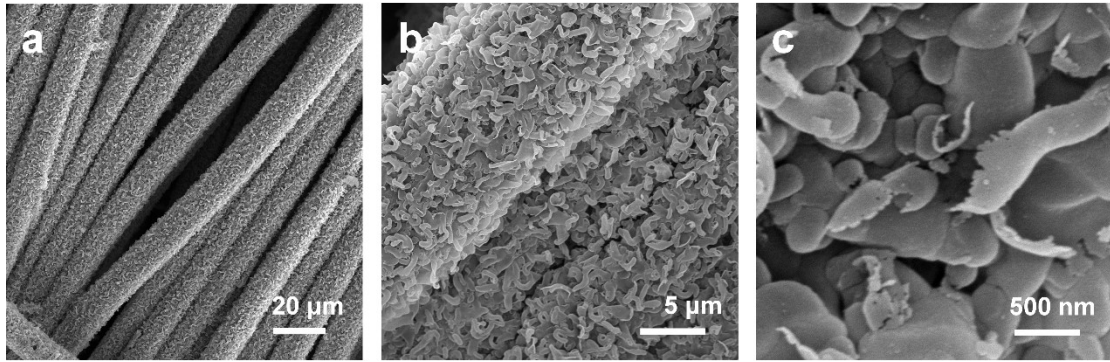


Figure S9. SEM images of Ni-MOF-74 NAs/CC-3 prepared with the addition of HMT (pH=3.45).

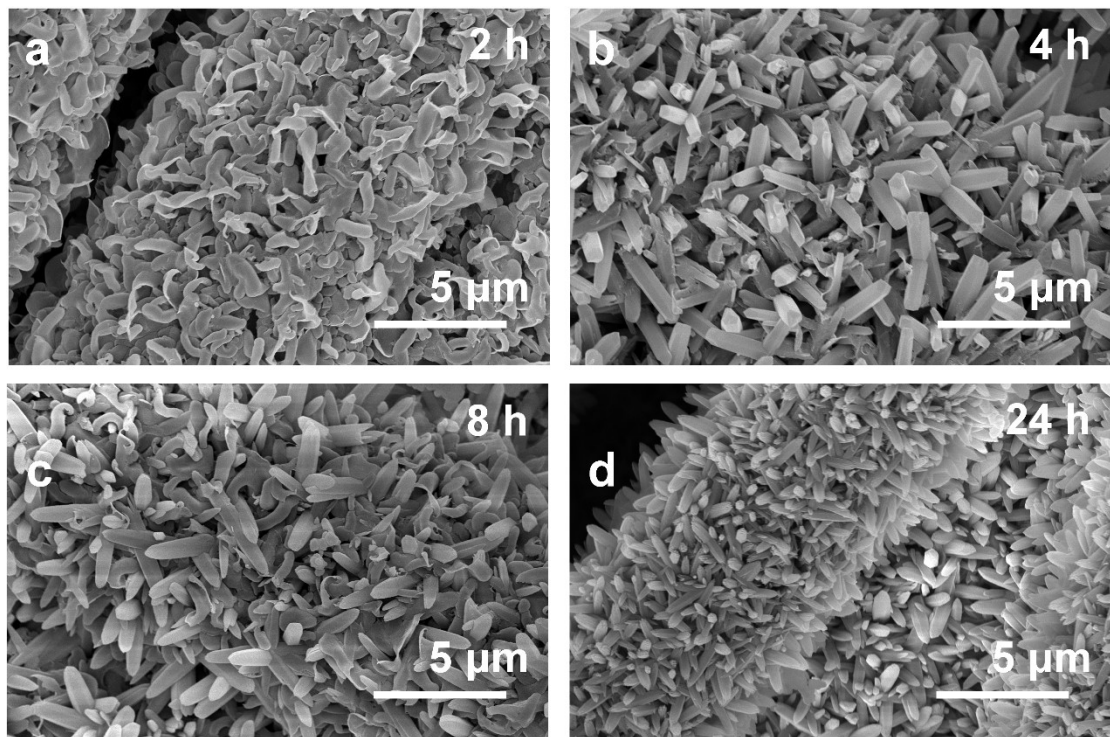


Figure S10. SEM images of Ni-MOF-74 NAs/CC-3 prepared under different reaction time (a-2h, b-4h, c-8h and d-24h).

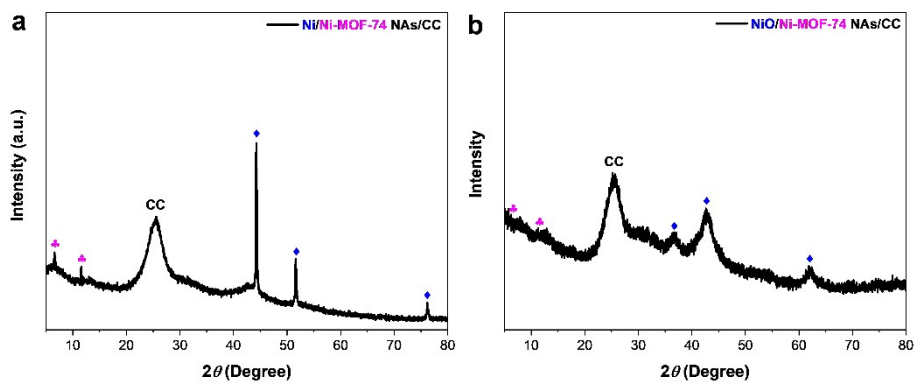


Figure S11. XRD patterns of Ni/Ni-MOF-74 NAs/CC (a) and NiO/Ni-MOF-74 NAs/CC (b), respectively.

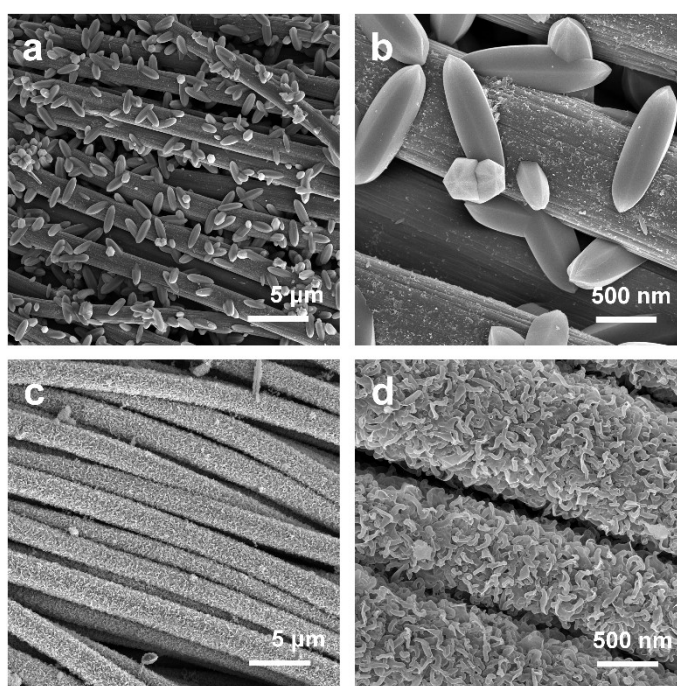


Figure S12. SEM images of (a, b) Ni/Ni-MOF-74 NAs/CC and (c, d) NiO/Ni-MOF-74 NAs/CC, respectively.

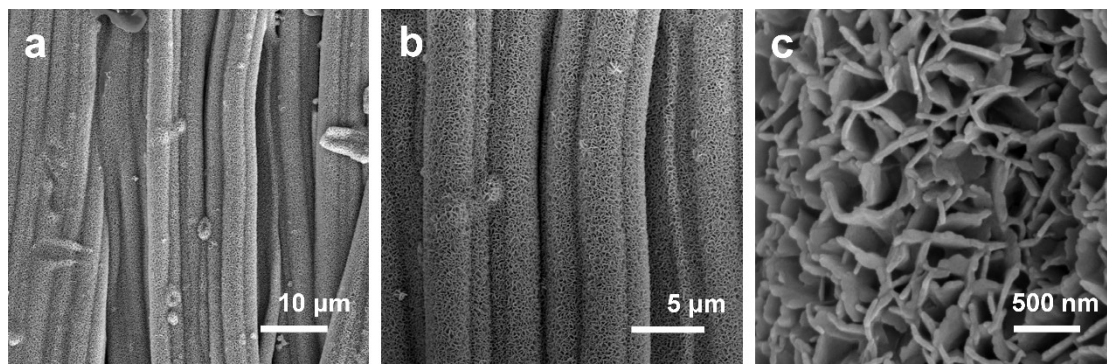


Figure S13. SEM images of Co(OH)₂ NAs/CC.

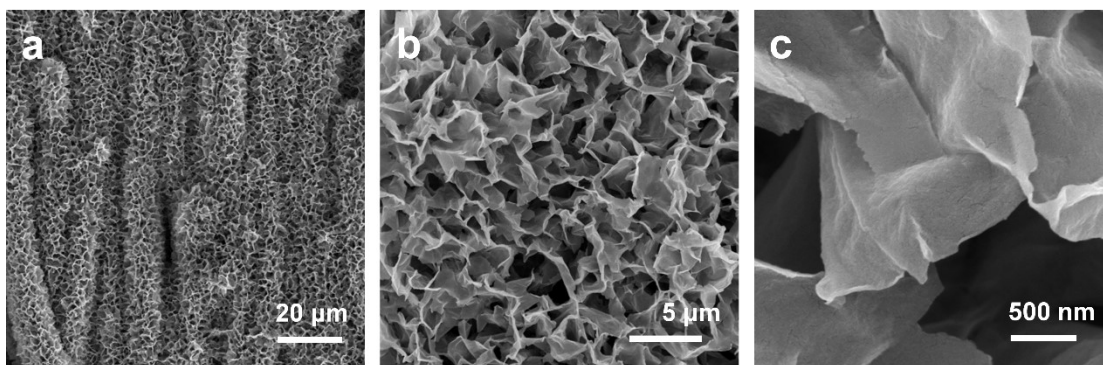


Figure S14. SEM images of $\text{Co}_{0.5}\text{Ni}_{0.5}(\text{OH})_2$ NAs/CC.

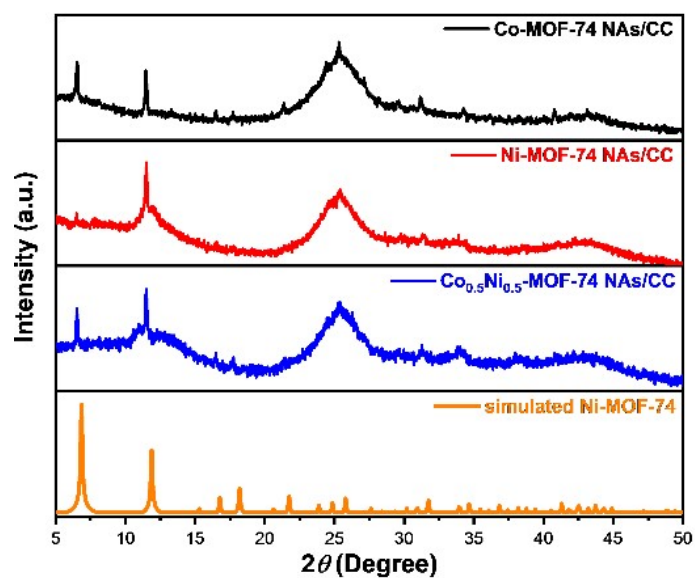


Figure S15. XRD patterns of Co-MOF-74 NAs/CC, Ni-MOF-74 NAs/CC and $\text{Co}_{0.5}\text{Ni}_{0.5}$ -MOF-74/CC, respectively.

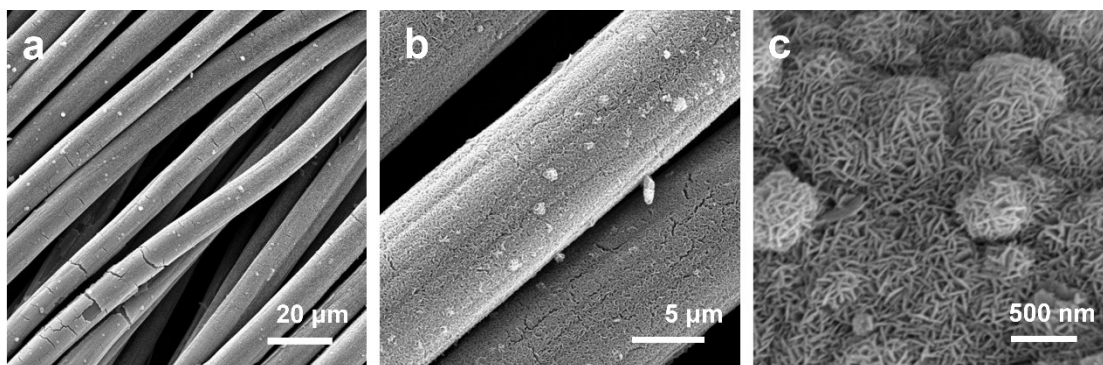


Figure S16. SEM images of Co-MOF-74 NAs/CC.

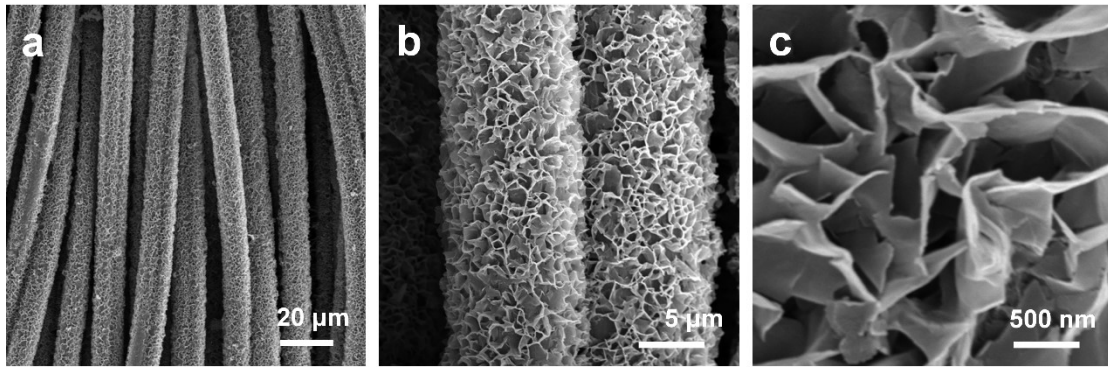


Figure S17. SEM images of $\text{Co}_{0.5}\text{Ni}_{0.5}\text{-MOF-74 NAs/CC}$.

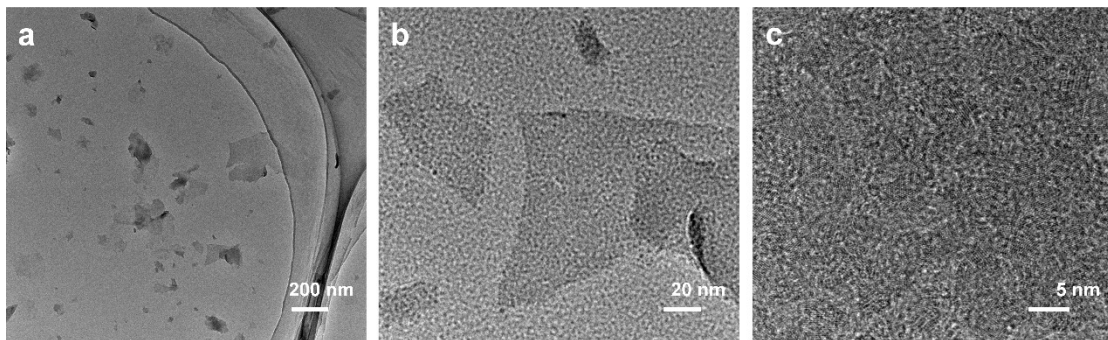


Figure S18. TEM images of Co(OH)_2 .

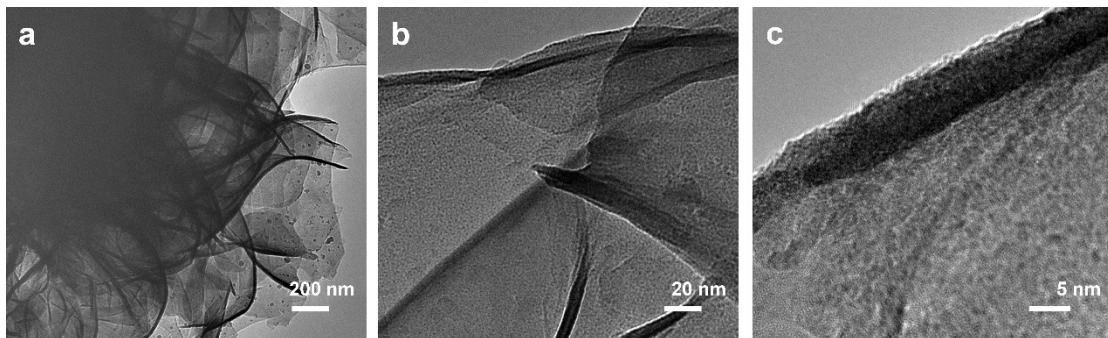


Figure S19. TEM images of Ni(OH)_2 .

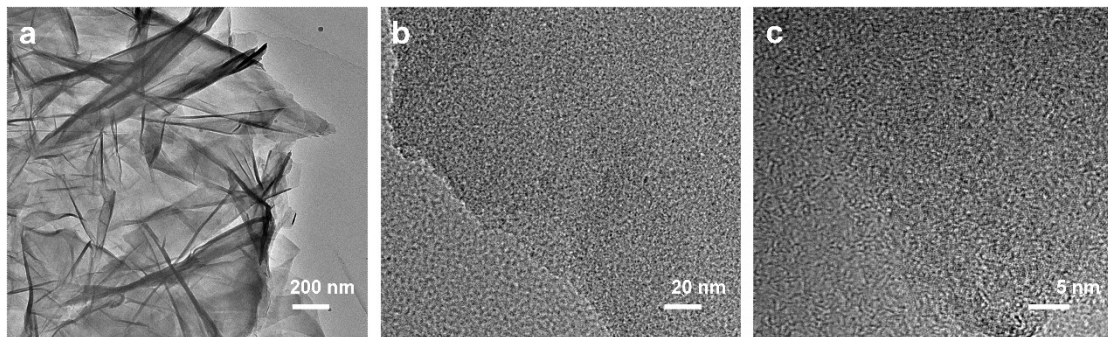


Figure S20. TEM images of $\text{Co}_{0.5}\text{Ni}_{0.5}(\text{OH})_2$.

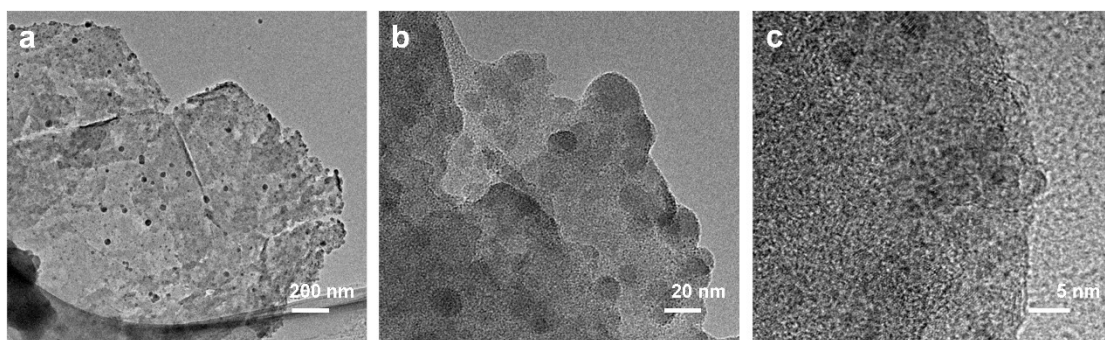


Figure S21. TEM images of Co-MOF-74.

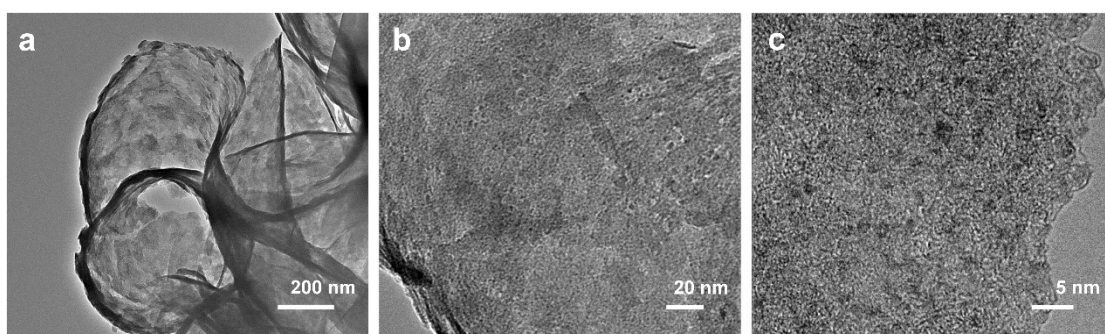


Figure S22. TEM images of Ni-MOF-74.

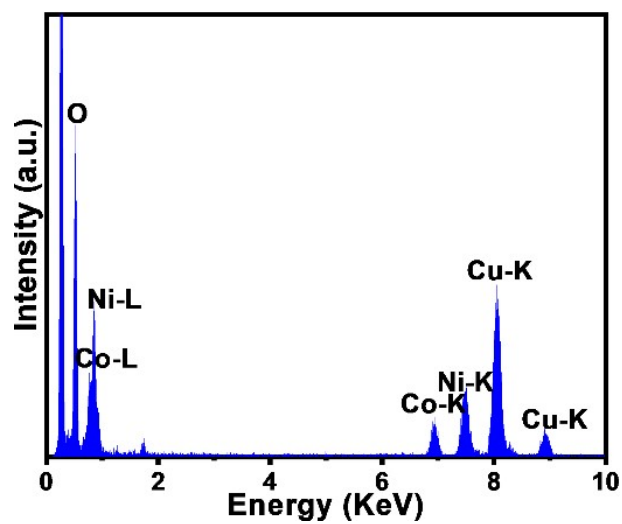


Figure S23. EDS plot of Co_{0.5}Ni_{0.5}-MOF-74.

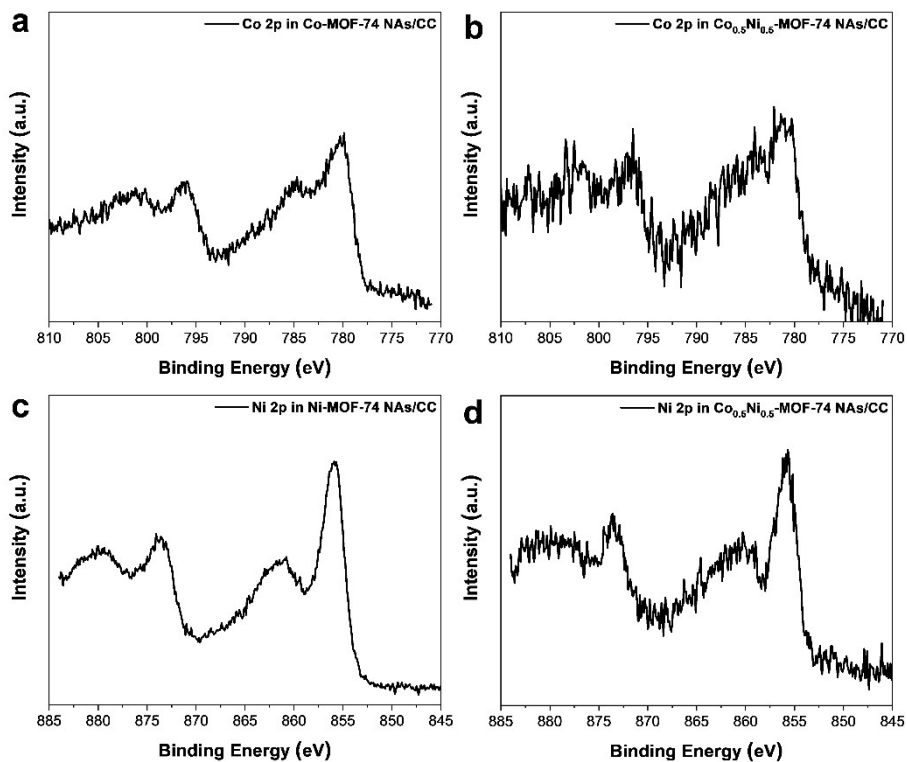


Figure S24. Full XPS spectra of Co/Ni 2p.

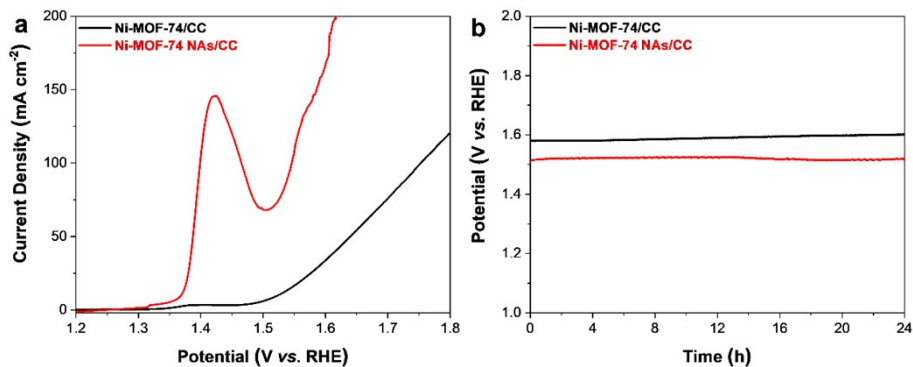


Figure S25. LSV (a) and CP (b) curves of Ni-MOF-74/CC and Ni-MOF-74 NAs/CC, respectively.

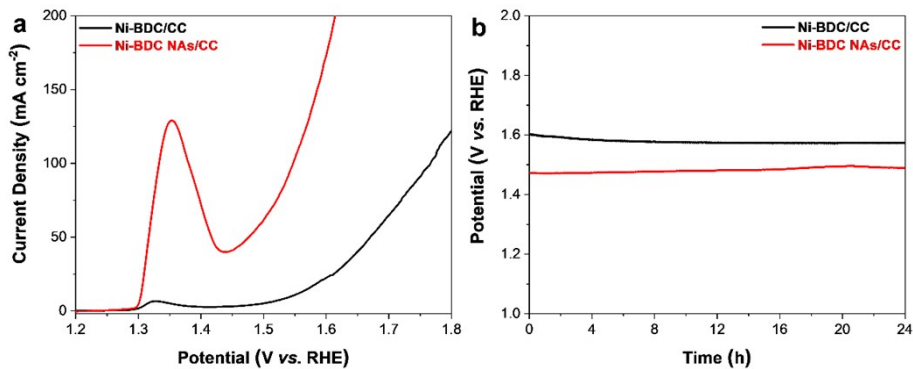


Figure S26. LSV (a) and CP (b) curves of Ni-BDC/CC and Ni-BDC NAs/CC,

respectively.

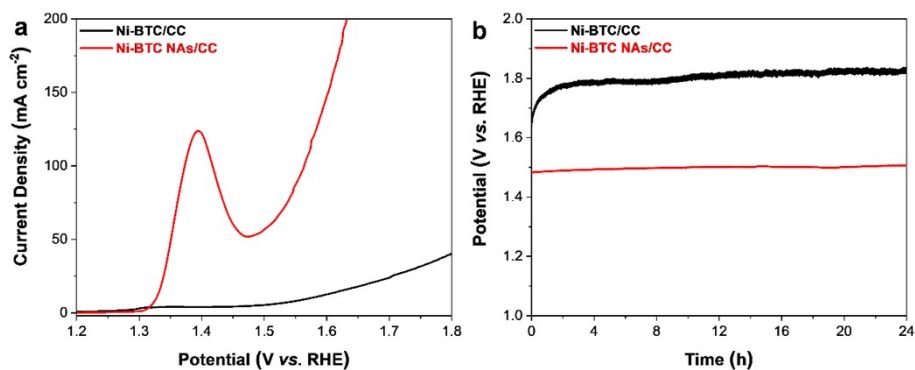


Figure S27. (a) LSV and (b) CP curves of Ni-BTC/CC and Ni-BTC NAs/CC, respectively.

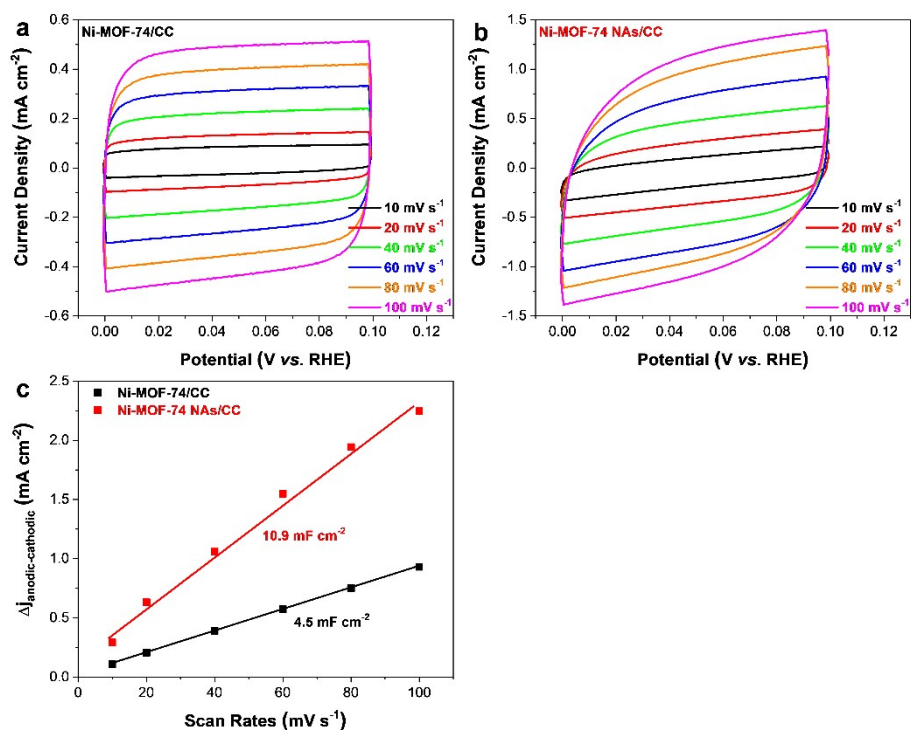


Figure S28. CVs of (a) Ni-MOF-74/CC and (b) Ni-MOF-74 NAs/CC with different scan rates, respectively. (c) The calculated differential current vs. scan rates at 0.049 V vs. RHE.

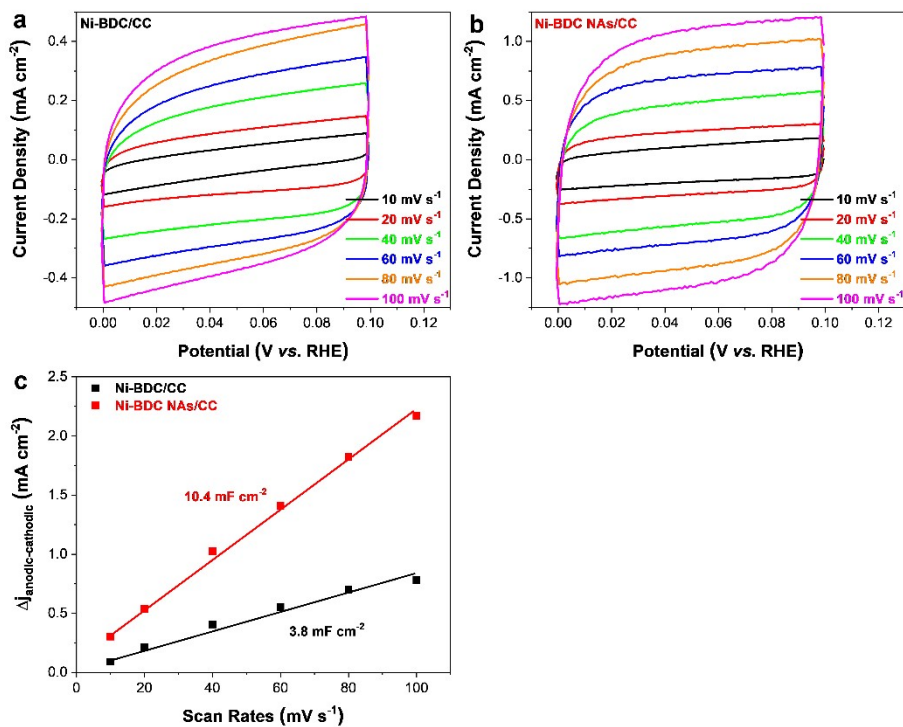


Figure S29. CVs of (a) Ni-BDC/CC and (b) Ni-BDC NAs/CC with different scan rates, respectively. (c) The calculated differential current vs. scan rates at 0.049 V vs. RHE.

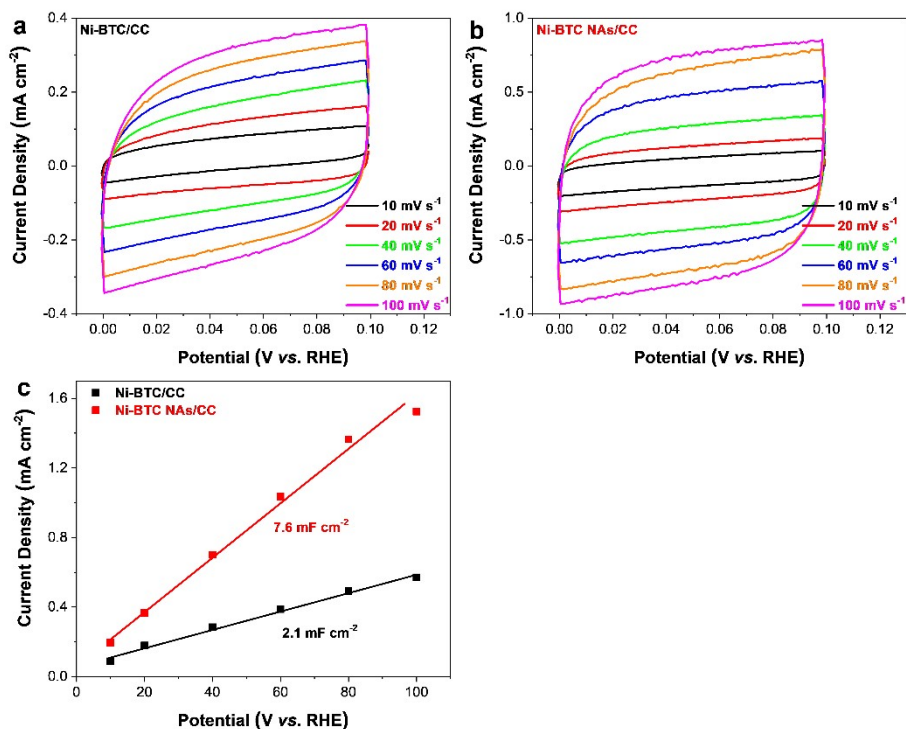


Figure S30. CVs of (a) Ni-BTC/CC and (b) Ni-BTC NAs/CC with different scan rates, respectively. (c) The calculated differential current vs. scan rates at 0.049 V vs. RHE.

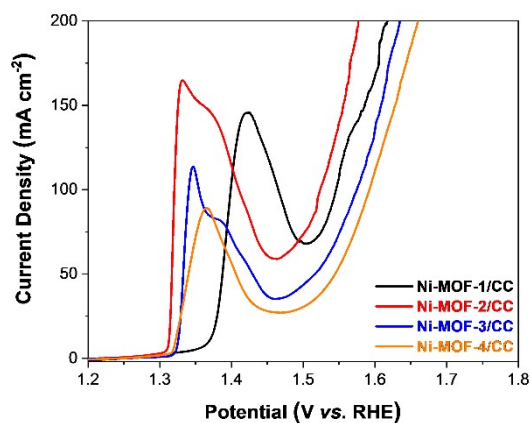


Figure S31. (a) LSV curves of Ni-MOF-74 NAs/CC-A (A=1, 2, 3 and 4).

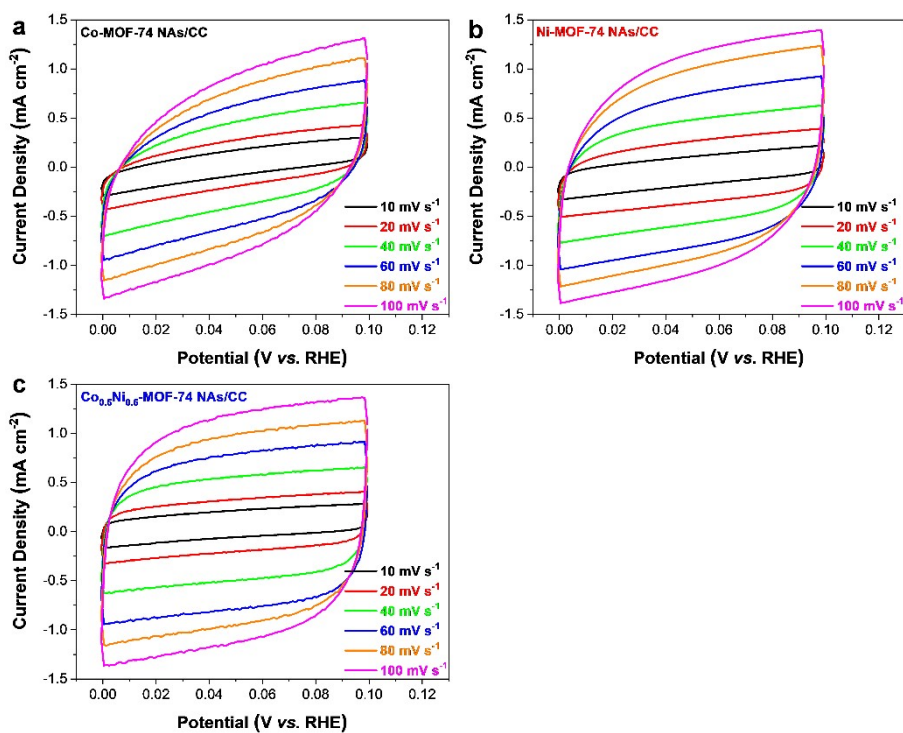


Figure S32. CVs of (a) Co-MOF-74 NAs/CC, (b) Ni-MOF-74 NAs/CC and (c) $\text{Co}_{0.5}\text{Ni}_{0.5}$ -MOF-74 NAs/CC with different scan rates, respectively.

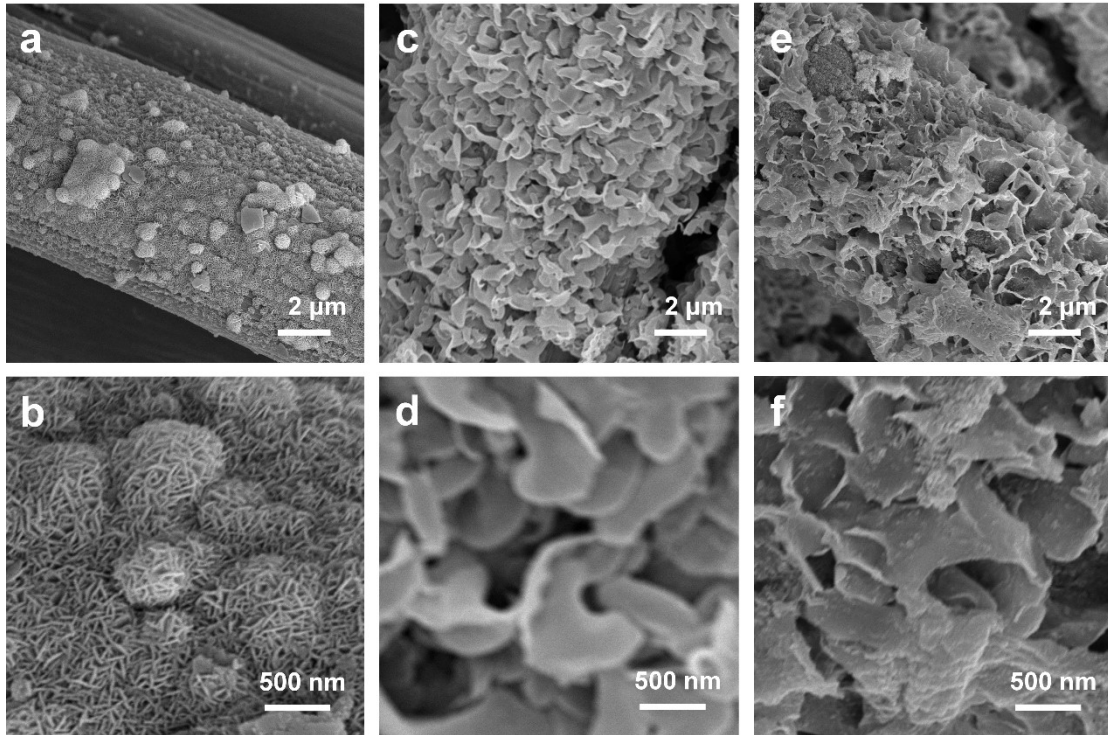


Figure S33. SEM images of Co-MOF-74 NAs/CC (a, b), Co-MOF-74 NAs/CC (c, d), Co-MOF-74 NAs/CC (e, f) after CP tests, respectively.

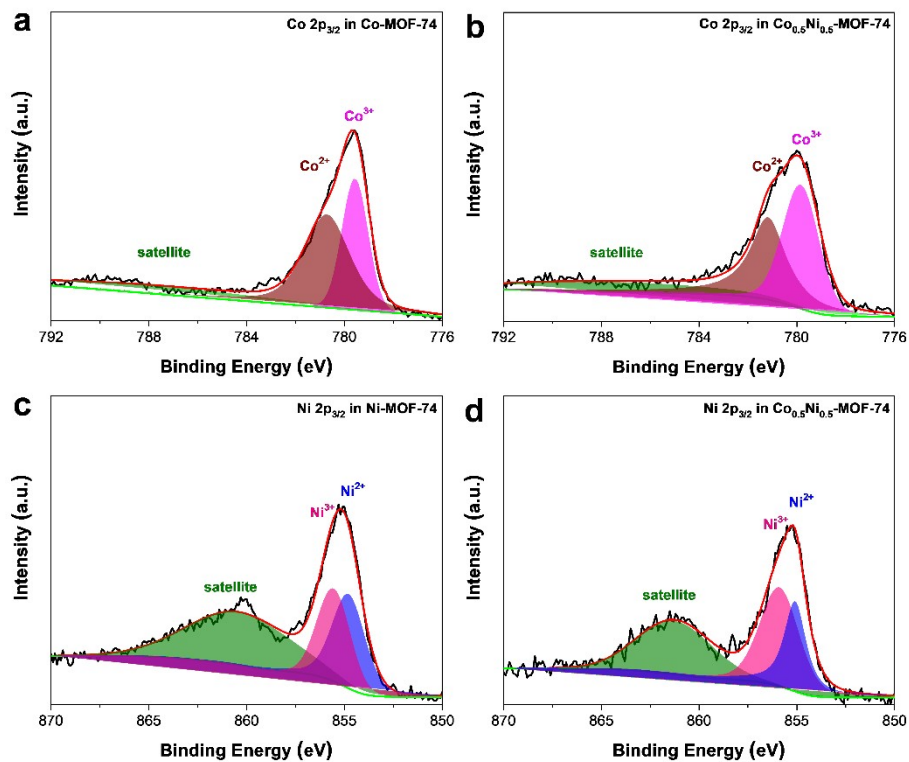


Figure S34. XPS of (a) Co 2p_{3/2} in Co-MOF NAs/CC, (b) Co 2p_{3/2} in Co_{0.5}Ni_{0.5}-MOF-74 NAs/CC, (c) Ni 2p_{3/2} in Ni-MOF-74 NAs/CC, (d) Ni 2p_{3/2} in Co_{0.5}Ni_{0.5}-MOF-74 NAs/CC after CP tests, respectively.

Table S1. Comparison of water oxidation activity in the electrolyte of 1 M KOH.

| Materials | electrolyte | Overpotential (mV) | References |
|--|-------------|--------------------|------------------|
| CoNi-MOF-74 NAs/CC | 1 M KOH | $\eta_{10}/244$ | This work |
| Fe-Ni ₃ S ₂ /NF ¹ | 1 M NaOH | $\eta_{100}/253$ | [1] |
| NiFe LDH/NF | 1 M KOH | $\eta_{10}/269$ | [2] |
| NiCo LDH/NG ² | 0.1 M KOH | $\eta_{145.3}/400$ | [3] |
| NiCo LDH/NF | 1 M KOH | $\eta_{10}/271$ | [4] |
| NiV LDH | 1 M KOH | $\eta_{27}/350$ | [5] |
| NiCr LDH/NF | 1 M KOH | $\eta_{100}/319$ | [6] |
| NiMn LDH/rGO ³ | 1 M KOH | $\eta_{10}/260$ | [7] |
| NiMn LDH | 1 M KOH | $\eta_{10}/350$ | [8] |
| NiMn LDH NS ⁴ | 0.1 M NaOH | $\eta_{20}/390$ | [9] |
| nNiFe LDH/NGF | 0.1 M KOH | $\eta_{10}/337$ | [10] |
| NiFe LDH/NF | 0.1 M KOH | $\eta_{30}/280$ | [11] |
| NiCu LDH/CC ⁵ | 1 M KOH | $\eta_{10}/290$ | [12] |
| NiZn LDH/N-rGO | 1 M KOH | $\eta_{10}/290$ | [13] |
| NiZn LDH nanocage | 1 M KOH | $\eta_{10}/290$ | [14] |
| NiFe-MOF/NF | 1 M KOH | $\eta_{10}/240$ | [15] |
| NiO/Ni-MOF/NF | 1 M KOH | $\eta_{50}/250$ | [16] |
| Fe ₂ O ₃ /Ni-MOF-74/CC | 1 M KOH | $\eta_{10}/264$ | [17] |
| Fe(OH) ₃ /Co-MOF-74/CC | 1 M KOH | $\eta_{10}/292$ | [18] |

1, NF, Ni foam; 2, NG, N-doped graphene; 3, rGO, reduced graphene oxide; 4, NS, nanosheet; 5, CC, carbon cloth;

References

- [1] N. Cheng, Q. Liu, A.M. Asiri, W. Xing, X. Sun, A Fe-doped Ni₃S₂ particle film as a high-efficiency robust oxygen evolution electrode with very high current density, *J. Mater. Chem. A*. 3 (2015) 23207–23212.
- [2] W. Chen, H. Wang, Y. Li, Y. Liu, J. Sun, S. Lee, J.-S. Lee, Y. Cui, In situ

- electrochemical oxidation tuning of transition metal disulfides to oxides for enhanced water oxidation, *ACS Cent. Sci.* 1 (2015) 244–251.
- [3] S. Chen, J. Duan, M. Jaroniec, S.Z. Qiao, Three-dimensional N-doped graphene hydrogel/NiCo double hydroxide electrocatalysts for highly efficient oxygen evolution, *Angew. Chem. Int. Ed.* 52 (2013) 13567–13570.
- [4] W. Liu, J. Bao, M. Guan, Y. Zhao, J. Lian, J. Qiu, L. Xu, Y. Huang, J. Qian, H. Li, Nickel–cobalt-layered double hydroxide nanosheet arrays on Ni foam as a bifunctional electrocatalyst for overall water splitting, *Dalt. Trans.* 46 (2017) 8372–8376.
- [5] K. Fan, H. Chen, Y. Ji, H. Huang, P.M. Claesson, Q. Daniel, B. Philippe, H. Rensmo, F. Li, Y. Luo, Nickel–vanadium monolayer double hydroxide for efficient electrochemical water oxidation, *Nat. Commun.* 7 (2016) 11981.
- [6] W. Ye, X. Fang, X. Chen, D. Yan, A three-dimensional nickel–chromium layered double hydroxide micro/nanosheet array as an efficient and stable bifunctional electrocatalyst for overall water splitting, *Nanoscale.* 10 (2018) 19484–19491.
- [7] W. Ma, R. Ma, J. Wu, P. Sun, X. Liu, K. Zhou, T. Sasaki, Development of efficient electrocatalysts via molecular hybridization of NiMn layered double hydroxide nanosheets and graphene, *Nanoscale.* 8 (2016) 10425–10432.
- [8] A. Sumboja, J. Chen, Y. Zong, P.S. Lee, Z. Liu, NiMn layered double hydroxides as efficient electrocatalysts for the oxygen evolution reaction and their application in rechargeable Zn–air batteries, *Nanoscale.* 9 (2017) 774–780.
- [9] R. Li, Y. Liu, H. Li, M. Zhang, Y. Lu, L. Zhang, J. Xiao, F. Boehm, K. Yan, One-Step Synthesis of NiMn-Layered Double Hydroxide Nanosheets Efficient for Water Oxidation, *Small Methods.* 3 (2019) 1800344.
- [10] C. Tang, H. Wang, H. Wang, Q. Zhang, G. Tian, J. Nie, F. Wei, Spatially confined hybridization of nanometer-sized NiFe hydroxides into nitrogen-doped graphene frameworks leading to superior oxygen evolution reactivity, *Adv. Mater.* 27 (2015) 4516–4522.
- [11] Z. Lu, W. Xu, W. Zhu, Q. Yang, X. Lei, J. Liu, Y. Li, X. Sun, X. Duan, Three-

- dimensional NiFe layered double hydroxide film for high-efficiency oxygen evolution reaction, *Chem. Commun.* 50 (2014) 6479–6482.
- [12] Y. Zheng, J. Qiao, J. Yuan, J. Shen, A. Wang, P. Gong, X. Weng, L. Niu, Three-dimensional NiCu layered double hydroxide nanosheets array on carbon cloth for enhanced oxygen evolution, *Electrochim. Acta.* 282 (2018) 735–742.
- [13] A. Nadeema, V.M. Dhavale, S. Kurungot, NiZn double hydroxide nanosheet-anchored nitrogen-doped graphene enriched with the γ -NiOOH phase as an activity modulated water oxidation electrocatalyst, *Nanoscale.* 9 (2017) 12590–12600.
- [14] S. Wang, J. Nai, S. Yang, L. Guo, Synthesis of amorphous Ni–Zn double hydroxide nanocages with excellent electrocatalytic activity toward oxygen evolution reaction, *ChemNanoMat.* 1 (2015) 324–330.
- [15] J. Duan, S. Chen, C. Zhao, Ultrathin metal-organic framework array for efficient electrocatalytic water splitting, *Nat. Commun.* 8 (2017) 15341.
- [16] Q. Hu, X. Huang, Z. Wang, G. Li, Z. Han, H. Yang, X. Ren, Q. Zhang, J. Liu, C. He, Unconventionally crafting defect-rich NiO nanoparticles within ultrathin metal-organic frameworks nanosheets to enable high-output oxygen evolution, *J. Mater. Chem. A.* 8 (2020) 2140–2146.
- [17] Z. Gao, Z.W. Yu, F.Q. Liu, Y. Yu, X.M. Su, L. Wang, Z.Z. Xu, Y.L. Yang, G.R. Wu, X.F. Feng, Ultralow-Content Iron-Decorated Ni-MOF-74 Fabricated by a Metal–Organic Framework Surface Reaction for Efficient Electrocatalytic Water Oxidation, *Inorg. Chem.* 58 (2019) 11500–11507.
- [18] Z. Gao, Z.W. Yu, F.Q. Liu, C. Yang, Y.H. Yuan, Y. Yu, F. Luo, Stable Iron Hydroxide Nanosheets@Cobalt-Metal–Organic–Framework Heterostructure for Efficient Electrocatalytic Oxygen Evolution, *ChemSusChem.* 12 (2019) 4623–4628.